EXTRACTION OF LINES FROM LASER POINT CLOUDS

Hermann Gross *, Ulrich Thoennessen

FGAN-FOM, Research Institute for Optronics and Pattern Recognition
76275 Ettlingen, Germany (gross,thoe)@fom.fgan.de

Commission III, WG III/3

KEY WORDS: Laser data, 3D point clouds, covariance of points, edge detection, line generation, eigenvalues, eigenvectors, momentum of inertia, segmentation

ABSTRACT:

Three dimensional building models have become important during the past for various applications like urban planning, enhanced navigation or visualization of touristy or historic objects. 3D models can increase the understanding and explanation of complex urban scenes and support decision processes. A 3D model of the urban environment gives the possibility for simulation and rehearsal, to "fly through" the local urban terrain on different paths, and to visualize the scene from different viewpoints. The automatic generation of 3D models using Laser height data is one challenge for actual research.
In many proposals for 3D model generation the process is starting by extraction of the border lines of man made objects. In our paper we are presenting an automatic generation method for lines based on the analysis of the 3D point clouds in the Laser height data. For each 3D point additional features considering the neighborhood are calculated. Invariance with respect to position, scale and rotation is achieved. Investigations concerning the required point density to get reliable results are accomplished. Comparing the new features with analytical results of typical point configurations provide discriminating features to select points which may belong to a line. Assembling these points to lines the borders of the objects were achieved. First results are presented.
Possibilities for the enhancement of the calculation of the covariance matrix by including the intensity of the Laser signal and a refined consideration of the neighborhood are discussed.

1. INTRODUCTION

Three-dimensional building models have become important during the past for various applications like urban planning, enhanced navigation or visualization of touristy or historic objects (Brenner et al., 2001). They can increase the understanding and explanation of complex scenes and support the decision process. The benefit for several applications like urban planning or the virtual sightseeing walk was demonstrated utilizing LIDAR data.

For decision support and operation planning the real urban environment should be available. In most cases the necessary object models are not present in the simulation data base. Especially in time critical situations the 3D models must be generated as fast as possible to be available for the simulation process.

Different approaches to generate the necessary models of the urban scene are discussed in the literature. Building models are typically acquired by (semi-) automatic processing of Laser scanner elevation data or aerial imagery (Baillard et al., 1999; Geibel & Stilla, 2000). For large urban scenes LIDAR data can be utilized (Gross & Thoennessen, 2005). Pollefeys (1999) uses projective geometry for a 3D reconstruction from image sequences. Fraser et al. (2002) use stereo approaches for 3D building reconstruction. Vosselman et al. (2004) describes a scan line segmentation method grouping points in a 3D proximity.

Airborne systems are widely used but also terrestrial Laser scanners are increasingly available. The latter ones provide a much higher geometrical resolution and accuracy (mm vs. dm) and they are able to acquire building facade details which are a requirement for realistic virtual worlds. Whereas in the orthogonal Nadir view of an airborne system the data can be interpreted as 2D image this is not possible for terrestrial Laser scanners.

We are presenting an approach for the segmentation of building parts like 3D edges. Analytical considerations give hints to extract these characteristic objects. We have realized and tested the detection of 3D edges as well as their approximation by lines. Also quality measures for the lines are determined. The capability of the algorithm is additionally demonstrated on the detection of overhead wires of a tram.

In chapter 2 the calculation of additional point features is described. The features are normalized with respect to translation, scale and rotation. The dependencies between covariance matrix and the tensor of momentum of inertia are discussed. Investigations on the sensitivity of the specified features deliver constraints concerning their usage.

In chapter 3 typical constellations of points are discussed and discriminating features are presented. Examples for the combination of eigenvalues and structure tensor are shown. For typical situations analytical feature values are derived.

The importance of a precise registration of Laser point clouds if different data sets have to be fused is illustrated in chapter 4.

The generation of lines is described in chapter 5. Points with the same eigenvectors are assembled and approximated by lines. Resulting 3D boundaries of objects are shown for different data sets.

In chapter 6 the possibilities using additional features are summarized. Outstanding topics and aspects of the realized method are discussed.

2. ADDITIONAL POINT FEATURES

A Laser scanner delivers 3D point measurements in an Euclidian coordinate system. For airborne systems mostly the height information is stored in a raster grid with a predefined resolution. Image cells without a measurement are interpolated by considering their neighborhood.
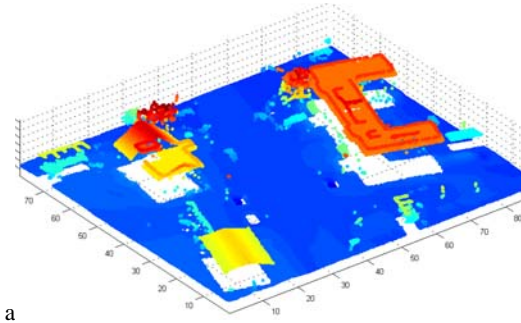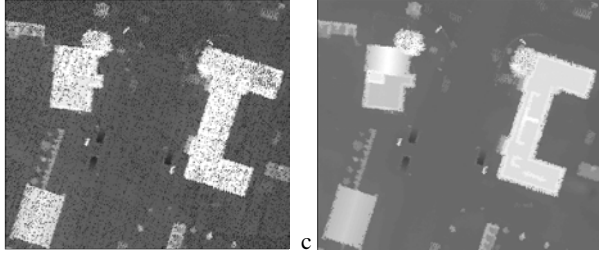
Figure 1. Point clouds from Toposys® Laser scanner
a) colored by height
Raster image based on point clouds:
b) without, c) with interpolated values

An example data set gathered by an airborne Laser scanner system as 3D points is shown in Figure 1a. The color corresponds to the height. A transformation to a raster image selecting the highest value for each pixel yields the Figure 1b. After filling missing pixels we are able to detect more details in Figure 1c. Due to the preprocessing steps the image does not represent the original 3D information anymore. The horizontal position is slightly different and some of the height values are calculated not measured. Additionally, sometimes more than one measurement for a resolution cell exists considering first and last echo or combining data of several measurement campaigns.

An example for a dense point cloud of a terrestrial Laser scanner is shown in Figure 2 representing the intensity of the signal.

Figure 2. Point clouds colored by intensity

In contrary to the airborne data the projection of terrestrial Laser data along any direction is not very reasonable. Especially the combination of airborne (Figure. 1) and terrestrial (Figure. 2) Laser scanning data requires directly the analysis in the 3D data.

2.1 Moments

A 3D spherical volume cell with radius R is assigned to each point of the cloud. All points in a spherical cell will be analyzed. 3D moments as described by Maas & Vosselman (1999) are discussed and improved.

In a continuous domain, moments are defined by:

$$m_{ijk} = \int_V x^i y^j z^k f(x,y,z) dv , \quad (1)$$

where $i, j, k \in \mathbb{N}$, and $i + j + k$ is the order of the moment integrated over a predefined volume weighted by $f(x,y,z)$.

As weighting function the mass density can be used. It reduces to a constant value if homogeneous material is assumed.

Another possibility is to use the intensity of the reflected Laser beam (s. Figure 2, Figure 11) as weighting function. Some aspects of using the intensity signal were discussed in (Jutzi et al., 2005).

We restrict the order of moments to $i + j + k \leq 2$. This delivers the weight, the center of gravity and the matrix of covariance. To be invariant against translation we calculate the center of gravity

$$\bar{x} = \frac{m_{100}}{m_{000}}, \quad \bar{y} = \frac{m_{010}}{m_{000}}, \quad \bar{z} = \frac{m_{001}}{m_{000}} \quad (2)$$

and the centralized moments

$$\bar{m}_{ijk} = \int_V (x - \bar{x})^i (y - \bar{y})^j (z - \bar{z})^k f(x,y,z) dv \quad (3)$$

with $\bar{m}_{000} = m_{000}$. Scale invariance may be achieved by

$$\tilde{m}_{ijk} = \frac{\bar{m}_{ijk}}{R^{i+j+k} \bar{m}_{000}} \quad (4)$$

We need two normalizations because $f(x,y,z)$ can take a different physical unit (other than length).

In the discrete case the integral (3) is approximated by the sum

$$\bar{m}_{ijk}(x_a, y_a, z_a) = \sum_{l=1}^{N} (x_l - \bar{x})^i (y_l - \bar{y})^j (z_l - \bar{z})^k f(x_l, y_l, z_l) \Delta v \quad (5)$$

including all points inside the sphere with radius R centered at an actual point $(x_a \quad y_a \quad z_a)$ with the constraint

$$\|(x_l \quad y_l \quad z_l) - (x_a \quad y_a \quad z_a)\| \leq R \quad (6)$$

Under the assumption that the incremental volume Δv is constant and due to the dependency of the moments from the number of points inside the sphere and the selected radius R we get the normalized moments

$$\tilde{m}_{ijk} = \frac{\bar{m}_{ijk}}{R^{i+j+k} \bar{m}_{000}} = \frac{\sum_{l=1}^{N} (x_l - \bar{x})^i (y_l - \bar{y})^j (z_l - \bar{z})^k f(x_l, y_l, z_l)}{R^{i+j+k} \sum_{l=1}^{N} f(x_l, y_l, z_l)} \quad (7)$$

For constant weighting function $f(x,y,z)$ as used in many cases we get

$$\tilde{m}_{ijk} = \frac{\sum_{l=1}^{N} (x_l - \bar{x})^i (y_l - \bar{y})^j (z_l - \bar{z})^k}{R^{i+j+k} N} \quad (8)$$

Neither the number of points nor the chosen physical unit for the coordinates, the radius and the weighting factor influences the values of the moments.

Finally we calculate for each point of the whole data set a symmetrical covariance matrix

$$M = \begin{pmatrix} \tilde{m}_{200} & \tilde{m}_{110} & \tilde{m}_{101} \\ \tilde{m}_{110} & \tilde{m}_{020} & \tilde{m}_{011} \\ \tilde{m}_{101} & \tilde{m}_{011} & \tilde{m}_{002} \end{pmatrix} \quad (9)$$

The calculation of the eigenvalues λ_i and eigenvectors $\vec{e}_i$ with $i = 1, 2, 3$ delivers features for each point. The eigenvalues are invariant concerning rotation.

If we calculate the tensor of momentum of inertia by

$$T = \left(\widetilde{m}_{200} + \widetilde{m}_{020} + \widetilde{m}_{002} \right) \begin{pmatrix} 1 & 0 & 0 \\ 0 & 1 & 0 \\ 0 & 0 & 1 \end{pmatrix} - M \qquad (10)$$

instead of the moments M of order two we will get the same eigenvectors. The sum of the eigenvalues belonging to the same eigenvector is constant for each eigenvector.

$$\lambda_i(M) + \lambda_i(T) = \widetilde{m}_{200} + \widetilde{m}_{020} + \widetilde{m}_{002} = const \quad \forall i = 1, 2, 3 \quad (11)$$

Due to the non contiguous (discrete) calculation of the moments the quality of the resulting numerical invariants can be discussed in a statistical (as moments M) or a physical (as moments of inertia T) way considering each point not only as a point but as a representative physical part of its surrounding.

2.2 Point distribution in 3D space

In this section we discuss the influence of the distribution of point measurements concerning the proposed features.
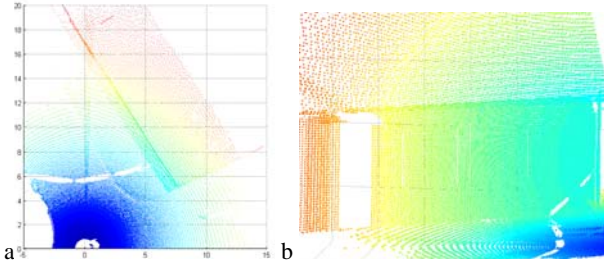
Figure 3.   Point clouds of a terrestrial Laser scanner:
a) vertical view, b) horizontal view; color indicates the distance to the sensor (blue=near, red=far away)

Figure 3 shows as an example for the dependency of the point density of the Zoller+Fröhlich Laser scanner concerning the distance to the sensor.

The comparable scan pattern of the Toposys sensor is shown in Figure 4a for a regular pattern and in Figure 4b for a wavy pattern. The point density in flight direction is usually much higher than in the perpendicular direction. In both cases there is no uniform distribution of the measured points.
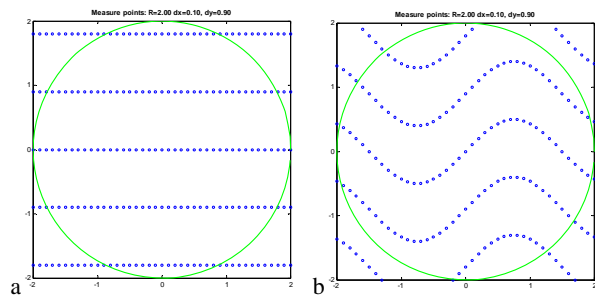
Figure 4.   Scan pattern similar to the Toposys Laser scanner:
a) regular pattern, b) wavy pattern

For non uniform distribution equations (1) and (5) imply to weight each point by the volume around this point without other points like inside a cell of a Voronoi diagram (Aurenhammer, 2000) or to correct the moments by integration over each cell of the diagram separately. To avoid such a time consuming but more precise calculation we have discussed the behavior of the eigenvalues of M dependent on the radius of the sphere and the density of the points. To investigate the behavior of the eigenvalues we have generated synthetically regular scans and also wavy scans (Figure 4) for a plane. After calculating covariance and eigenvalues taking all points inside the green circle we consider the ratio λ_2 / λ_1 of the second and the greatest eigenvalue. The third eigenvalue is $\lambda_3 = 0$.
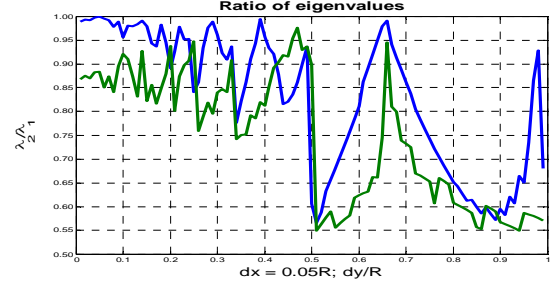
Figure 5.   Ratio of λ_2 / λ_1 dependent on the smaller point density dy / R: blue: regular pattern; green: wavy pattern

Figure 5 shows the ratio of the non zero eigenvalues dependent on the density of the points in the y-direction. Nearly the same behavior is calculated for both the regular and the wavy scan. The ratio for the regular pattern (blue) is slightly greater than for the wave pattern (green). The variations of the function are caused by the digitalization (Figure 4). For $dy / R < 0.5$, dy point distance in y-direction, we got acceptable results. Weighting each point by the same factor we have to select the radius of the sphere as $R > 2dy$ (two times of the largest point distance.) Under this constraint λ_2 / λ_1 is greater than 0.75 (e.g. $dx = 0.1m$ $dy = 0.5m$ $\Rightarrow$ $R > 1m$).

3.   FILTERING OF POINTS

After calculation of the covariance matrix for each point in the data set considering a local environment defined by a sphere we have additional features for each point.

S	Type	λ_1	λ_2	λ_3
	Isolated point	0	0	0
	End of a line	$\dfrac{1}{12}$	0	0
	Line	$\dfrac{1}{3}$	0	0
	Half plane	$\dfrac{1}{4}$	$\dfrac{1}{4}\left(1 - \dfrac{64}{9\pi^2}\right) = 0.07$	0
	Plane	$\dfrac{1}{4}$	$\dfrac{1}{4}$	0
	Quarter plane	$\dfrac{1}{4}\left(1 - \dfrac{2}{\pi}\right) = 0.09$	$\dfrac{1}{4} + \dfrac{1}{2\pi} - \dfrac{32}{9\pi^2} = 0.05$	0
	Two planes	$\dfrac{1}{4}$	$\dfrac{1}{8}$	$\dfrac{1}{8} - \dfrac{8}{9\pi^2} = 0.03$
	Three planes	$\dfrac{1}{6}\left(1 - \dfrac{1}{\pi}\right) = 0.11$	$\dfrac{1}{6}\left(1 - \dfrac{1}{\pi}\right) = 0.11$	$\dfrac{1}{6}\left(1 + \dfrac{2}{\pi}\right) - \dfrac{2^6}{3^3\pi^2} = 0.03$

Table 1.   Eigenvalues for some typical situations

These features are the center of gravity, the distance between center of gravity to the point, the eigenvectors, the eigenvalues and the number of points inside the sphere. They can be used for determination of object characteristics.

Table 1 shows the eigenvalues of the covariance matrix of some special point configurations. The first six rows present 2D cases the last two 3D ones.

The ratios are based on typical situations and analytically calculated. For an ideal line two eigenvalues are zero and one of it is greater than zero. For straight edges at the border of a half-plane one eigenvalue is zero and the ratio of

$\frac{\lambda_2}{\lambda_1} = \frac{9\pi^2 - 64}{9\pi^2} = 0.28$ shows a significant difference between

the both non zero eigenvalues. If we are looking for points inside a plane we have to compare the eigenvalues $\lambda_1 = \lambda_2 = 0.25 \quad \wedge \quad \lambda_3 = 0$ with the values for a plane. For the edge points at the intersection line of two orthogonal planes the

ratios are $\frac{\lambda_2}{\lambda_1} = 0.5$ and $\frac{\lambda_3}{\lambda_1} = 0.5 - \frac{32}{9\pi^2} = 0.14$.

Figure 6a shows all points with eigenvalues satisfying the criteria for planes. The color indicates the object height. In Figure 6b only the edge points are drawn corresponding to Table 1 row 4.

a

b
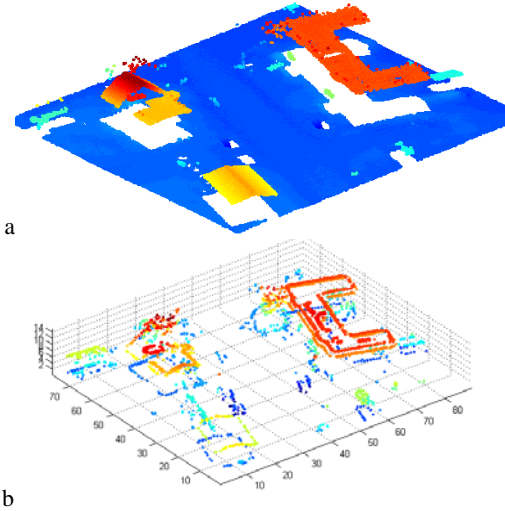
Figure 6.   a) Points identified as plane points
           b) Points with one high and two small eigenvalues

For object classification especially for region growing West (2004) uses the following features which depends on the eigenvalues:

$$\text{Structure Tensor Omnivariance } = \sqrt[3]{\prod_{i=1}^{3} \lambda_i} \qquad (12)$$

$$\text{Structure Tensor Anisotropy } = \frac{\lambda_1 - \lambda_3}{\lambda_1} \qquad (13)$$

$$\text{Structure Tensor Planarity } = \frac{\lambda_2 - \lambda_3}{\lambda_1} \qquad (14)$$

$$\text{Structure Tensor Sphericity } = 1 - \text{Anisotropy} = \frac{\lambda_3}{\lambda_1} \qquad (15)$$

$$\text{Structure Tensor "Eigenentropy" } = -\sum_{i=1}^{3} \lambda_i \log(\lambda_i) \qquad (16)$$

$$\text{Structure Tensor Linearity } = \frac{\lambda_1 - \lambda_2}{\lambda_1} \qquad (17)$$

a

b
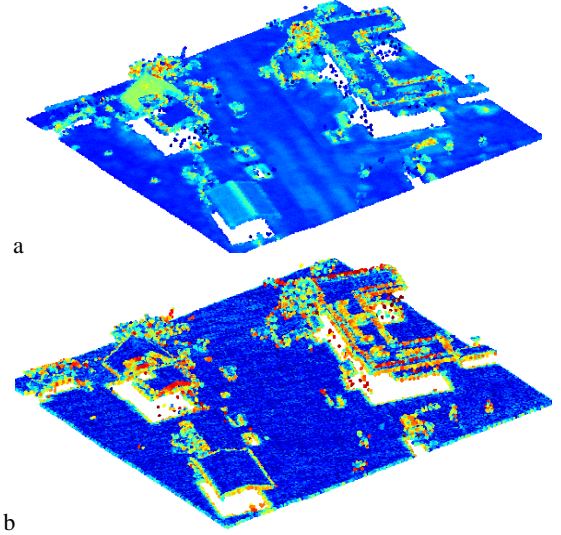
Figure 7.   Points marked by a) Omnivariance b) Linearity

Figure 7 shows the points classified and colored by the features a) Omnivariance and b) Linearity. A detailed analysis of these features for point classification is under investigation.

4. REQUIREMENT FOR REGISTRATION

The enhancement of resolution is possible combining multiple scans of the same scene. We have investigated this approach for airborne Laser scan data (Toposys). Especially the reconstruction of gabled roofs was considered. A precise registration of the data sets is necessary.

The application of the filter process mentioned before delivered the result shown in Figure 8a. A detailed analysis shows some discrepancy in the registration of different scan data. Viewing along the ridge of the gabled roof, Figure 8a, demonstrates the gap between two flights.

a   b
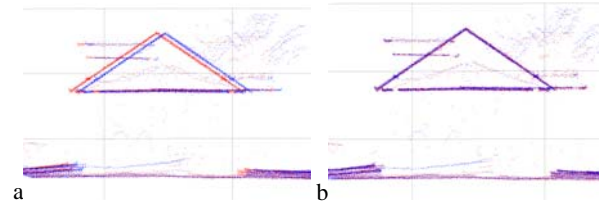
Figure 8.   Gabled roof a) before and b) after fine registration

Using the Iterative Closest Point (ICP) algorithms (Besl 1992, Fitzgibbon, 2001) the registration was refined (Figure 8b). This method uses data of two point clouds inside a common region and determines translation, rotation and scaling to minimize the distance between the point clouds. Based on the transformed data acceptable eigenvalues for the classification of the planes of the gabled roof are achieved.

5. LINE GENERATION

All points marked as edge point may belong to a line. These points are assembled to lines by a grouping process. We consider the greatest eigenvalue λ_1 and its eigenvector $\overline{e}_1$. Consecutive points with a similar eigenvector, lying inside a small cylinder are grouped together and approximated by a line. Let Cl be the set of all points of the cloud. Starting with any point $\overline{p} \in Cl$ with eigenvector $\overline{e}_1^p$ as feature. This point is

called the trigger point. Now we are looking for all points $\overline{c}$ and determine the set

$$C = \left\{ \overline{c} \in Cl \left\| \overline{e_1^p} \circ \overline{e_1^c} \right| > \text{min\_cos} \right\} . \quad (18)$$

This set contains all points with nearly the same or opposite direction for the first eigenvector tested comparing the inner product of two vectors against a given threshold min_cos. We construct a line through the trigger point along its first eigenvector:

$$\overline{g} = \overline{p} + \mu \overline{e_1^p} \quad (19)$$

The scalar components for $\overline{c} \in C$ to each eigenvector are

$$\mu_i(\overline{c}, \overline{p}) = (\overline{c} - \overline{p}) \circ \overline{e_i^p} . \quad (20)$$

Due to the normalization of the eigenvectors these components describe the distances along each direction. The distance of the point $\overline{c}$ to the line is

$$d(\overline{c}, \overline{p}) = \sqrt{\mu_2^2(\overline{c}, \overline{p}) + \mu_3^2(\overline{c}, \overline{p})} \quad (21)$$

Let $D = \left\{ \overline{c} \in Cl \middle| d(\overline{c}, \overline{p}) \leq \text{max\_d} \right\}$ be the set of edge points inside the cylinder given by $\overline{g}$ with the given radius max_d. The intersection $GP = C \cap D$ includes all edge points with nearly the same first eigenvector as the trigger point and not far away from the straight line given by the trigger point and its first eigenvector.

Collinear edges of different buildings in a row may belong to $GP(\overline{p})$. Therefore we examine the contiguity of the points in the neighborhood of $\overline{p}$. The scalar values $\mu_1(\overline{c}, \overline{p})$ describe the projection of the points onto the straight line. Let $\mu s(\overline{c}, \overline{p})$ a sorted list of the $\mu_1(\overline{c}, \overline{p})$. Because $\mu s(\overline{p}, \overline{p}) = 0$, we have to search for gaps defined by an acceptable value max_gap on the left and right side of zero. $\mu s_L \leq 0$ is the left boundary and $\mu s_R \geq 0$ is the right boundary if

$$\mu s_{L-1} + \text{max\_gap} < \mu s_L \ \wedge \ \mu s_R + \text{max\_gap} < \mu s_{R+1}$$
$$\wedge \ \ \mu s_{j-1} + \text{max\_gap} \geq \mu s_j \ \ \forall L < j \leq R \quad (22)$$

Let $GPs = \left\{ \overline{c} \in GP \middle| \mu s_L \leq \mu(\overline{c}, \overline{p}) \leq \mu s_R \right\}$ the set of points along the straight line without gap with respect to $\overline{p}$. For determination of the line we calculate the mean values $\overline{cm} = \frac{1}{n} \sum_{\overline{c} \in GPs} \overline{c}$ where n is the number of points in GPs. The direction of the line is given by the eigenvector $\overline{e_1}$ belonging to the greatest eigenvalue of the covariance matrix CM. The elements of the matrix are

$$cm_{ij} = \frac{1}{n} \sum_{\overline{c} \in GPs} (x - xm)^i (y - ym)^j (z - zm)^k \quad (23)$$

where

$$(x \quad y \quad z) = \overline{c} \ \text{ and } \ (xm \quad ym \quad zm) = \overline{cm} \quad (24)$$

The straight line is described by $\overline{xl} = \overline{cm} + \mu \overline{e_1}$. Start point and endpoint are given by

$$\overline{xa} = \overline{cm} + \min_{\overline{c} \in GPs} (\overline{c} \circ \overline{e_1}) \overline{e_1} \ \text{ and } \ \overline{xe} = \overline{cm} + \max_{\overline{c} \in GPs} (\overline{c} \circ \overline{e_1}) \overline{e_1} \ (25)$$

The length of the line is

$$L = \left\| \overline{xe} - \overline{xa} \right\| \quad (26)$$

The eigenvalues of CM can be normalized by $v_i = \frac{\lambda_i}{L^2}$ to be independent from length. These normalized eigenvalues are reasonable for a quality assessment of the lines. The same process is repeated for all points not assigned to a line until each point belongs to a line or can not generate an acceptable line.

Figure 9 shows the results of the line generation for the data set shown in Figure 1. The color indicates the height of the lines. The eaves as well as the ground plan of the buildings are approximated by lines. For the detection of the ridge of the saddle roof we have to use other thresholds for the eigenvalues especially for roofs with small inclination.
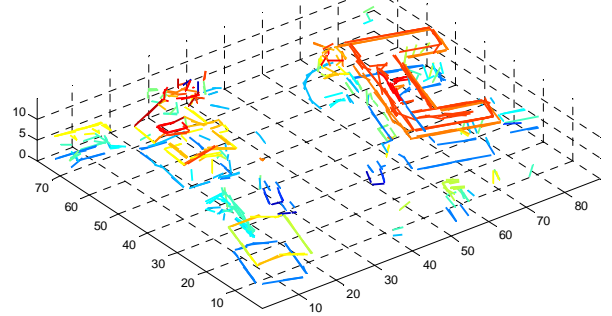
Figure 9.   Lines generated from edge points

For the scene from Figure 3 we got the approximation lines shown in Figure 10. The ridge line, the contour lines at the bottom of the building and the boundary lines of the door are detected.
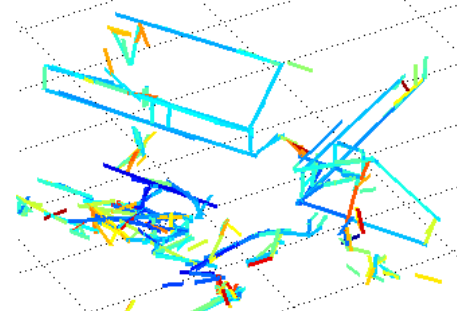
Figure 10. Lines generated from edge points for the point clouds of a terrestrial Laser scanner (s. Figure 3) colored by the 1. eigenvalue
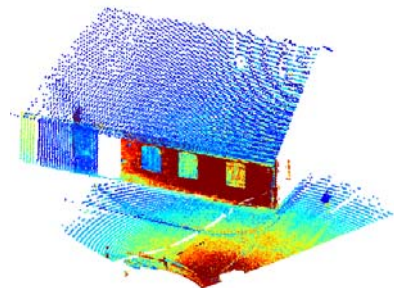
Figure 11. Building of Figure 3 colored by intensity

Considering the intensity of the Laser scanner signal of the same scene (Figure 11) we will investigate the reconstruction of windows. More tests have to be accomplished to stabilize the method.

The proposed method delivers not only edges of buildings but also the overhead wires of tramways in a city. For data from the Toposys sensor Figure 12 displays the Last- and First-Echo and Figure 13 shows the generated lines of the power lines and the support wires.
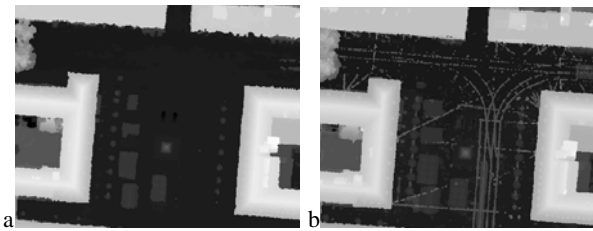
Figure 12. LastEcho and FirstEcho of a city scene
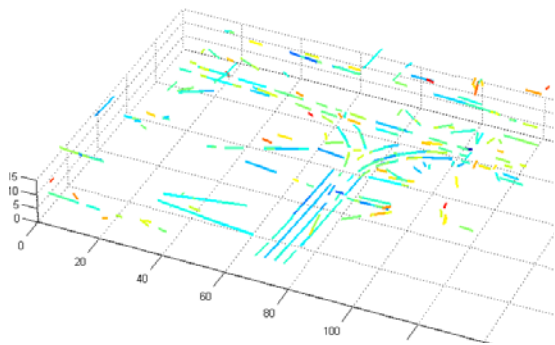
Figure 13. Lines generated from edge points for overhead wires

6. CONCLUSION AND OUTLOOK

Laser scanner systems gather directly 3D information. For data reduction and visualization the data sets are transformed often to a raster grid interpolating gaps. Due to this step the original 3D data is tampered.

For terrestrial Laser scan data this method is more difficult to apply and tampering error may be larger. Additional problems will appear if we want to fuse airborne and terrestrial data sets. We propose the exploitation of the original 3D point clouds.

Additional features for each point of the cloud are calculated from the covariance matrix including all neighbor points. The neighborhood is defined by a sphere. The quality of the resulting eigenvalues and the eigenvectors of the matrix depends on the resolution and the number of points inside the sphere. For different resolutions of different scan directions these values are discussed. Based on this investigation the radius of the sphere can be calculated by a function of the resolution. The new features are invariant with respect to position, rotation and scale.

The additional features are appropriate for classification of the points as edge, corner, plane or tree points. For some typical situations analytically determined eigenvalues are opposed to calculated eigenvalues of real data for comparison. The greatest eigenvalue is used for filtering edge like points.

The described method for generation of lines combines consecutive points with the same eigenvector inside a small cylinder without any gap. The presented results are promising.

Further investigations are planned concerning the fusion of the data on basis of the point clouds and/or on a higher level of lines. For the filtering process features derived from the eigenvalues (12)-(17) should be tested on different kind of data to get a robust point classification.

A further topic is the construction of planes assembling plane like points.

A calculation of the covariance matrix which is adapted to the resolution should be investigated and may deliver better results. This process is expensive and should be tested on several data sets.

LITERATURE

Aurenhammer F., Klein R., 2000, Voronoi Diagrams, Ch. 5 in *Handbook of Computational geometry*, Ed. J.-R. Sack and J. Urrutia, Amsterdam Netherland: North-Holland, pp. 201-290

Baillard, C., Schmid, C., Zisserman, A. and Fitzgibbon A., 1999. Automatic line matching and 3D reconstruction from multiple views. In: *ISPRS Conference on Automatic Extraction of GIS Objects from Digital Imagery*, Vol. 32.

Besl P.J., McKay N.D. 1992. A Method for registration of 3D shapes, *IEEE Trans. Pattern Anal. and Machine Intell.* 14 (2), 239-256

Brenner, C., Haala, N. and Fritsch, D., 2001. Towards fully automated 3D city model generation. In: *E. Baltsavias, A. Grün and L. van Gool (eds), Proc. 3rd Int. Workshop on Automatic Extraction of Man-Made Objects from Aerial and Space Images*.

Fitzgibbon A. W., 2001. Robust Registration of 2D and 3D Point Sets, *Proceedings of the British Machine Vision Conference*, 2001, 662-670

Fraser C. S., Baltsavias E., Gruen A., 2002. Processing of IKONOS Imagery for Submetre 3D Positioning and Building Extraction. *ISPRS Journal of Photogrammetry & Remote Sensing* 56, 177-194

Geibel R., Stilla U., 2000. Segmentation of Laser-altimeter data for building reconstruction: Comparison of different procedures. *International Archives of Photogrammetry and Remote Sensing*. Vol. 33, Part B3, 326-334

Gross H., Thoennessen U., 2005. 3D Modeling of Urban Structures. Joint Workshop of ISPRS/DAGM Object Extraction for 3D City Models, Road Databases, and Traffic Monitoring CMRT05, *Int. Archives of Photogrammetry and Remote Sensing*, Vol. 36, Part 3/W24, pp. 137-142

Jutzi B., Neulist J., Stilla U., 2005. Sub-Pixel Edge Localization Based on Laser Waveform Analysis, ISPRS WG III/3, III/4, V/3 *Workshop "Laser scanning 2005", Enschede, the Netherlands*, pp. 109-114

Maas H., Vosselman G., 1999. Two algorithms for extracting building models from raw Laser altimetry data, *ISPRS Journal of Photogrammetry & Remote Sensing 54*, pp. 153-163

Pollefeys M., 1999. Self-Calibration and Metric 3D-Reconstruction from Uncalibrated Image Sequences, PhD-Thesis, K. U. Leuven

Vosselman, G. et al., 2004. Recognizing structure in Laser scanner point clouds. Int. *Archives of Photogrammetry, Remote Sensing and Spatial Information Sciences*, Vol. 46, part 8/W2, Freiburg, Germany, pp. 33-38.

West, K. F. et al., 2004. Context-driven automated target detection in 3-D data. *Automatic Target Recognition XIV, edited by Firooz A. Sadjadi, Proceedings of SPIE* Vol. 5426, pp. 133-143.